

Hybrid Metal Foams: Experimental Observations and Phenomenological Modelling

A. Jung, S. Diebels

Metal foams are a very interesting class of microheterogeneous, cellular, lightweight materials which are often used as kinetic energy absorber. In this study open cell metal foams consisting of a 3D network of interconnected pores have been coated with nanocrystalline nickel via an electrodeposition technique. The resulting hybrid foams were submitted to several uniaxial and biaxial tests, where not only the stress-strain response but also the energy absorption capacity, size effects and damage behaviour were investigated.

Metal foams exhibit localized deformation states under inelastic strain conditions that cause localisation of damage in crushing zones with a thickness of several pore layers. Building up of the crushing zones has been studied by using the digital image correlation (DIC) technique. The abovementioned strain localisation causes stress fluctuations which can be seen in macroscopic stress-strain diagrams. In this work a new modelling approach has been developed that allows for explicit consideration of such microstructural effects in a phenomenological way. The model is based on a qualitative phenomenological and rheological spring model. The size of a representative volume element (RVE) is equal to the thickness of a crushing zone and consists of several springs where each spring corresponds to one pore layer. By introducing a rheological model for the RVE in this way the constitutive equations still contain fundamental parameter but these are motivated by the microstructure, whereas the phenomenological model is able to account for microstructural effects.

1 Introduction

Metal foams are a very interesting class of porous, cellular bio-inspired materials, which mimic the framework of natural load-bearing structures like bones. They consist of a three-dimensional network of stochastically distributed pores. Based on their special structure, metal foams are microheterogeneous materials. For a phenomenological description of the material properties of metal foams it is suitable to define three hierarchical structural levels with different length scales (see Figure 1).

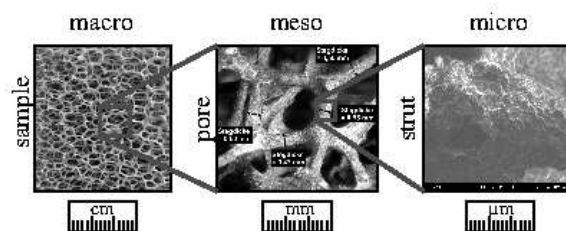


Figure 1: The three hierarchical levels of microheterogeneous materials like open cell metal foams.

On each hierarchical level the foam can be divided into sublevels, which are homogeneous on the sublevel. According to this homogenization, the mechanical properties on one hierarchical level only depend on the inhomogeneities of its sublevel. The characteristic length scale on the macro scale covers several pores up to the whole sample. On the macro scale the foams are regarded as a continuum, hence, it is not possible to investigate damage and deformation mechanisms on the macro scale. This could be done on the meso scale. Here the characteristic length is the average length of one pore diameter and in the order of several millimeters. The meso scale is characterised by the shape, thickness and length of the pores. A further resolution of the struts leads to the microstructure. The microstructure describes the structure of the struts, the grain size, voids, micro pores and inclusions in the struts. The fields of application for metal foams is very broad. Based on their high specific stiffness to weight ratio, they

are used as light weight construction materials (Ashby (1983); Ashby et al. (2000)). Their special stress-strain diagram offers the opportunity as energy absorber e.g. in transportation industry (Banhart et al. (1997); Banhart and Baumeister (1998); Banhart (2001)). Based on the large internal surface area, a third field of application comprises functional applications as heat exchanger, sound absorber, catalyst support and electromagnetic shielding (Ashby (1983); Ashby et al. (2000); Banhart (1999); Lefebvre et al. (2008)). Mostly, metal foams are only good in one of these three fields of application and hence, they have to compete with established materials which are in most cases also cheaper. In order to make them ready to the market, metal foams must be good in two or even all of the three fields of application such that they provide multifunctional usage. The foams are usually made of aluminium because of the low density, low melting point and the comparatively low costs, but the low strength of aluminium is a further disadvantage.

Metal foams show a special tripartite stress-strain diagram (see Figure 2). The first part is a nearly linear elastic region according to Hooke's law. This part is terminated by the so called plastic collapse stress (PCS), the point, where the first pore layer in the foam begins to buckle. The PCS is followed by a long stress plateau. Based on the gradually collapse of the remaining porous layer, the stress is nearly constant over a large strain regime. After the collapse of all pores there is the densification of the material and it behaves like a bulk metal but without tensile stiffness. The complete stress-strain diagram can be described by ideal elasticity in the first regime, ideal plasticity in the second and contact of the struts in the third regime. Whereas bulk metals show nearly similar compression and tensile strength, metal foams offer a distinct compression behaviour but show only a low tensile strength.

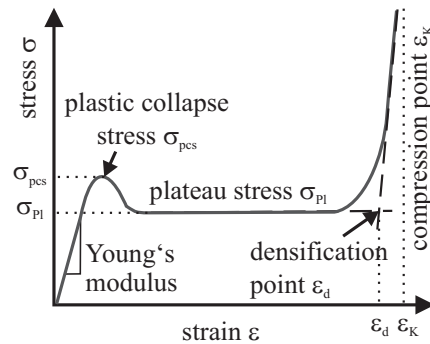


Figure 2: Schematic stress-strain diagram of metal foams.

A further distinctive feature of metal foams are size effects. Size effects arise if the intrinsic length scales like the pore size are in the same order of magnitude as the extrinsic length scales like the sample size (Abrate (1997); Ashby et al. (2000); Onck et al. (2001); Andrews et al. (2001); Tekoglu et al. (2011); Chen and Fleck (2002)). According to Ashby et al. (2000), if the sample consists of less than eight pores, decreasing sample sizes lead to increased PCS and plateau stress of the foams under compression. This size effect arises from edge effects. At the boundaries of the foam which are not in contact with the load plates of the testing machine, there are struts with free ends. In foams, each strut is connected with five other struts. The struts in the boundary regions are only connected with three other struts. Under compressive load the struts with the free ends in the boundary regions remain stress-free. Also neighbouring cells to the stress-free boundary layers show reduced strength. Struts in the foam are constrained in all directions in space by neighbouring cells and hence possess high stiffness and high strength. With increasing sample size, there is a reduced fraction of the weakened boundary layer of the whole sample and thus there is a reduced contribution of the weakened boundaries to the macroscopic material properties of the foams. The ratio of sample height to pore size strongly influences the mechanical properties of metal foams. For infinitely high samples the foam properties reach a kind of saturation point and the foam behaves like a classical continuum.

In this study we tried to improve the mechanical properties and the multifunctionality of open cell aluminium metal foams by a nanocrystalline coating with nickel. The mechanical properties and the size effect have been characterised in quasi-static compression tests and biaxial shear compression tests. Micro-macro identification and the role of length scale have been extensively studied in the literature and are not limited to foams. But mostly, there is a more mathematical treatment to describe the special situations (Alibert et al. (2003); Diebels and Geringer (2013); Ferretti et al.; Jänicke et al. (2013)). Based on the experimental observations of this work, we developed a simple one-dimensional phenomenological model which is able to qualitatively describe the experimental observations.

2 Materials and Methods

2.1 Synthesis of Hybrid Metal Foams by Electrodeposition

Electrodeposition is a very versatile technique for the coating of materials. It is commonly used for the coating of planar substrates or the outer surface of three-dimensional objects. Based on diffusion problems and electromagnetic shielding effects, coating of metal foams is a quite complex task, because not only the outer surface but also the inner surface have to be coated. Hence a special cathode-anode arrangement was developed by Jung et al. (2009, 2010, 2011). The foams were plated with nanocrystalline nickel using a commercial nickel sulfamate electrolyte (Enthone GmbH, Langenfeld, Germany) at current densities of 1.5 mA/cm^2 . The exact preparation procedure was mentioned in a previous work of Jung et al. (2009, 2010, 2011).

2.2 Mechanical Characterization

Cubic samples of pure aluminium foams and hybrid foams with different coating thicknesses with an edge length of 40 mm have been tested in quasi-static compression tests using an universal testing machine INSTRON 4204. The tests were performed at strain rates of $5 \times 10^3 \text{ s}^{-1}$. In order to determine the Young's modulus during the deformation of the foams, combined shear-compression tests with periodically shear unloading have been accomplished with pure aluminium foams ($40 \times 40 \times 120 \text{ mm}^3$) at a shear rate of $7 \times 10^4 \text{ s}^{-1}$ using a shear load frame RS5 of Ltd. GIESA.

3 Experimental Results

3.1 Quasi-static Compression Tests

Figure 3 outlines the stress-strain diagrams of 10 ppi aluminium and Ni/Al-hybrid foams. Increasing coating thicknesses leads to a linear increase in the PCS and in the plateau stress. In general, the pore collapse occurs by bending and buckling of the struts of the foam. The improvement is based on a strengthening of the foams' bending and buckling stiffness by the coating due to the three times higher Young's modulus of nickel in comparison to aluminium. In bending and buckling the maximal stresses in tension and compression are located in the boundary of the struts, in the center there is the stress-free neutral fibre. Hence, the coating is a density optimized strengthening of the foams.

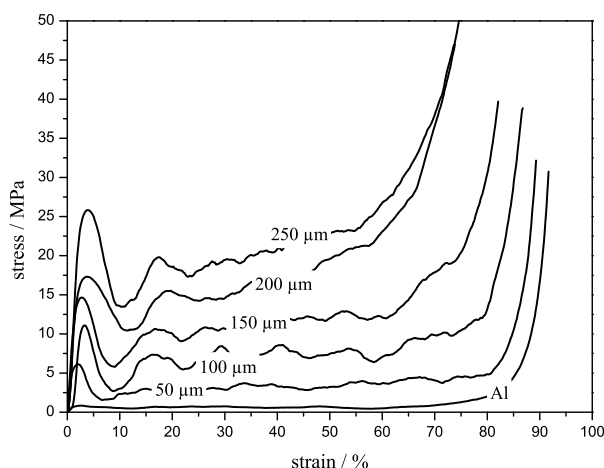


Figure 3: Stress-strain diagrams of 10 ppi aluminium and Ni/Al-hybrid foams as function of the coating thickness.

Size effects have been also investigated by quasi-static compression tests. Figure 4 (a) outlines the stress-strain diagrams of 10 and 30 ppi foams which are of the same dimensions and Figure 4 (b) the stress-strain diagrams of 10 and 30 ppi foams which possess the same ratio of pore size to sample size, meaning that they have the same number of pores in load direction.

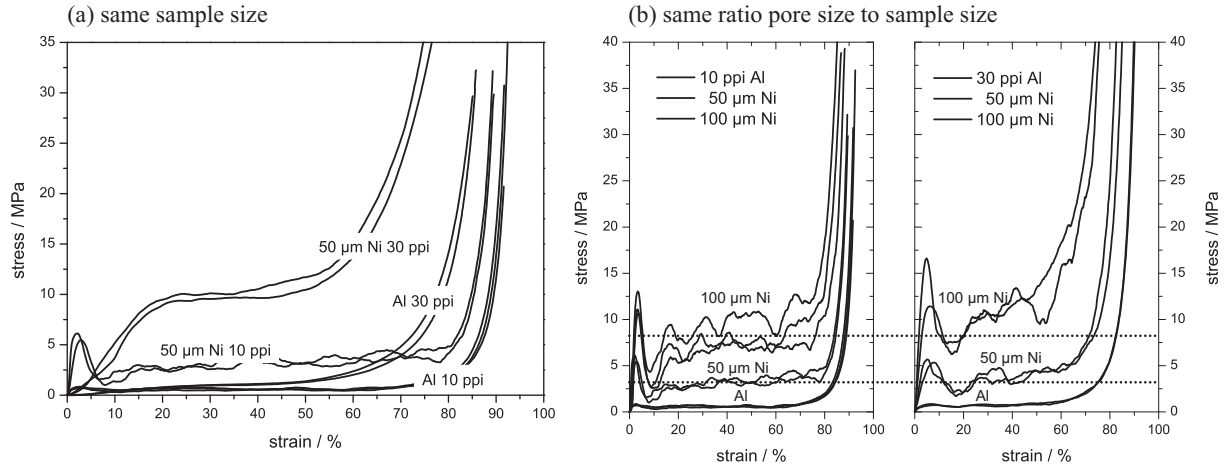


Figure 4: Size effects: Stress-strain diagrams of 10 and 30 ppi aluminum and Ni/Al-hybrid foams. (a) same sample size, (b) same ratio of pore size to sample size.

As explained in Chapter 1, the mechanical properties of cellular materials like foams are strongly dependent on the pore size. Figure 4 (a) shows that a reduction in the pore size without a change in the sample size leads to increased strength and plateau stress and it also changes the shape of the stress-strain diagram. The increased number of pores causes the disappearance of the PCS-peak. In Figure 4 (b) there is the comparison of 10 and 30 ppi foams with the same ratio of the pore size to sample size. In this case, for both pore sizes, there is a pronounced PCS-peak visible and the foams show a quite similar stress-strain characteristic.

3.2 Combined Shear-Compression Tests

Combined shear-compression tests with imposed constant compressive loadings of 1.4, 2.5 and 3.0 kN, respectively, are shown in Figure 5. The periodical shear unloading was performed in order to determine the Young's modulus of the foams at different strains.

The unloading leads to the formation of hysteresis loops. These are based on the pseudo-elastic behaviour of metal foams. Although the macroscopical deformation in the first part of the stress-strain diagrams looks linear elastic, there are localised plastic deformations in some struts which lead to a reduced stiffness. Thus, it is important to determine the Young's modulus during the unloading and not during the loading. For different imposed loadings, there is a change in the deformation mechanism from shear-dominated for an imposed loading of 1.4 kN to compression dominated for imposed loadings of 2.5 kN and higher. This is presented in Figure 5 (a) where there are several minima in shear force for imposed loadings of 2.5 and 3.0 kN. The subsidence (see Figure 5 (b)) corresponds to the vertical displacement of the sample during the shear tests. Jumps in the subsidence correlate with the spontaneous collapse of a pore layer and a decrease in the shear forces. Figure 5 (c) presents the evolution of the Young's modulus with increasing shear displacement. The behaviour of the Young's modulus is in good accordance to the behaviour of the shear force with increased displacement. The stiffness increases with increasing displacement except that there is a decrease in the shear force by a collapsing pore layer. This increased stiffness could be feasible explained by a rule of mixtures

$$E = \nu_1 E_1 + \nu_2 E_2 \quad (1)$$

where ν_1 is the volume fraction and E_1 the Young's modulus of the strut material and ν_2 the volume fraction and E_2 the Young's modulus of the pore fluid, i.e. air. Increasing displacements lead to the compression of the foams and to the removal of pores, hence the volume fraction of the strut material increases up to 100% in the case of the compression point.

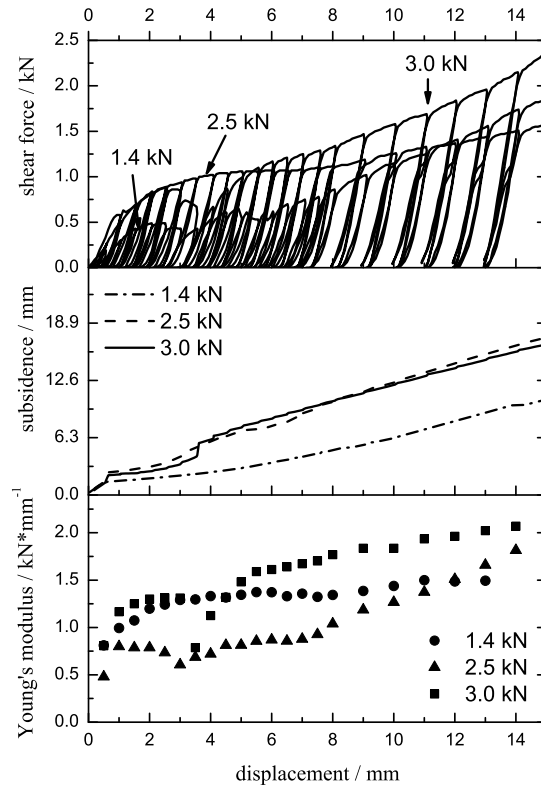


Figure 5: Combined shear-compression tests for pure aluminium foams.

4 Phenomenological Material Model with Material Degradation

4.1 Model Requirements

In Figure 3 and Figure 6 (a) the stress-strain diagrams display several oscillations in stress during the plateau phase. Figure 6 shows that this is based on the mesoscopic deformation mechanism, the buckling of the struts. As seen from Figure 6 (c) this buckling leads to localised strain and the formation of crushed deformation bands. Each oscillation is coupled with the damage of one porous layer.

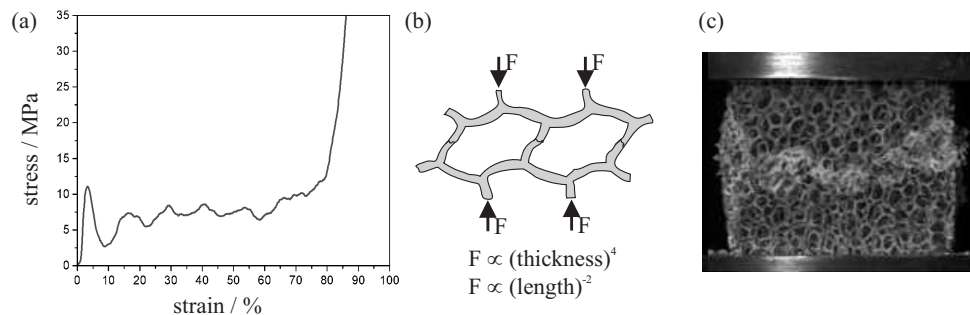


Figure 6: (a) stress-strain diagram of 100 μm Ni/Al hybrid foam, (b) schematic view of the mesoscopic buckling mechanism, (c) digital image correlation with localised strain bands.

Based on the experimental observations in Chapter 3 and the abovementioned deformation mechanisms, a material model to describe the mechanical behaviour of metal foams has to provide different behaviour under tension and compression, compressibility, hardening and increased stiffness with increasing strain, strain localisation expressed in oscillations in stress and also size effects. In this context the model has to describe both kinds of size effects: softening with increasing sample size and with increasing pore size.

4.2 Phenomenological and Rheological Model

A phenomenological model to describe the model requirements can be summarized in the following gedankenexperiment. There must be a case-by-case analysis for the three different regims in the stress-strain diagram of a metal that describes a kind of macroscopical material degradation. In the first part, the foam behaves ideally linear elastic and offers similar stiffness under compression and tension. The porous structure will be simply reversibly stretched or compressed. The total volume of the foam is composed of the pore volume and the solid volume of the struts. The second part of the stress-strain diagram, the plateau phase is macroscopically described by ideal plasticity but in reality it is not plasticity. On the mesoscopic and microscopic level, respectively, the ideal plasticity arises from a damage of the struts. According to the damage, the foam offers increased compression stiffness with increasing number of collapsed pore layers but totally lose its tensile stiffness after the first pore collapse. Losing the tensile stiffness is based on the gedankenexperiment that in the plateau regime at least one pore layer is collapsed. The remaining is a loose conglomerate of crushed struts. On the one hand, there is no solid material connection between the struts in the crushing zone, hence tensile loading on this conglomerate separates the sample and no stress can be evaluated. But on the other hand, further compression on such a damaged foam leads to further crushing of pore layers and thus to increased stiffness by the irreversible loss of the pore volume, whereas the solid volume of the struts remains unchanged. In the contact area of the stress-strain diagram, the former foam structure consists of a loose conglomerate of crushed pore layers. This means, the pore volume is irreversibly, completely removed. Under compression the remaining solid volume, build by the crushed struts, behaves like a non-cellular material but without tensile stiffness. This gedankenexperiment is schematically outlined in Figure 7.

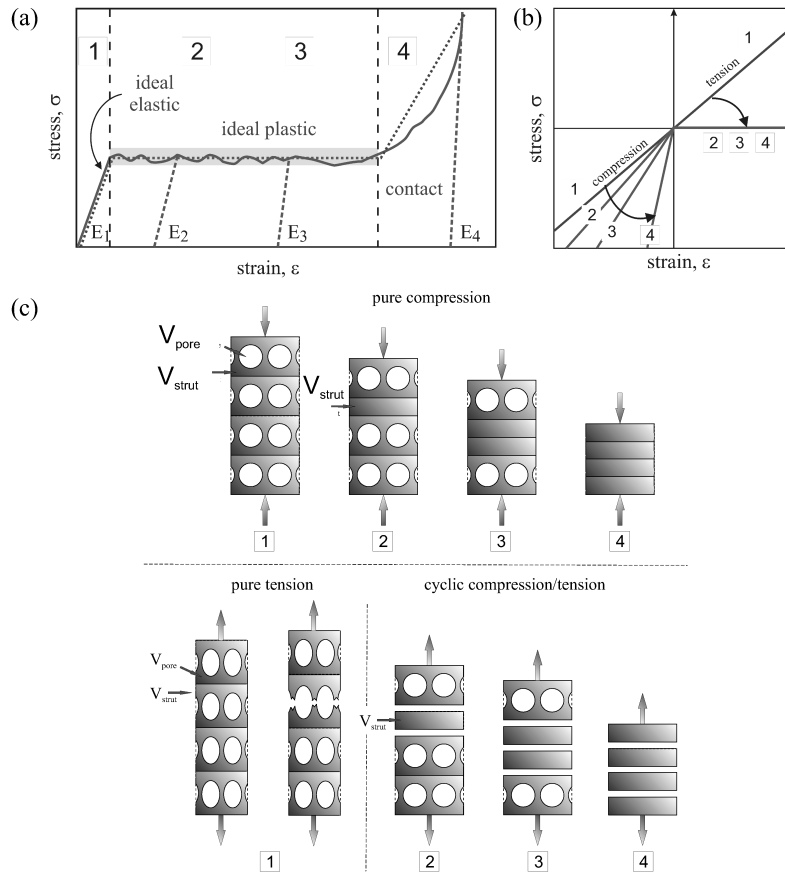


Figure 7: (a) idealised stress-strain diagram of a metal foam, (b) stiffness characteristics, (c) gradual evolution of damage and crushing zones under compression, tension and of compressively predamaged foams.

In the following, a one dimensional rheological spring model will be evaluated, which is able to accomplish all requirements of Chapter 4.1 and qualitatively describe the ideal stress-strain diagram of a metal foam (see Figure 7) but uses a microstructural approach for the phenomenological based fundamental parameter of the model. A schematical overview of the proposed model for three different load cases presented for two pore layers is given in Figure 8. Case 0 describes two different stress-free states. The first state is the unloaded foam, no external stress is applied. The second stress-free state consists of a totally undeformed second pore layer and a totally crushed

first pore layer. L is the overall length of the foam, L_i denotes to the length of one pore layer. The length Q_i is an internal length which is introduced to describe the new overall length after a pore collapse. Case 1 corresponds to a stress state which is just before the critical yield stress of the first pore layer, with other words, just under the critical collapse stress. Δ belongs to an infinitesimally small amount of stress. Hence the case 2 describes a stress state, where the stress is just higher than the critical collapse stress. After the pore collapse, there is a redistribution of the applied strain in the individual pore layers by conservation of the overall strain. This pore model can be translated into a rheological spring model (Figure 8 (b)), whereas each pore layer is represented by a spring. In case 1 before the pore collapse, the stiffness of all springs is E_i^- and there is an equal distribution of strain (ε_i^-) between the springs. After the pore collapse in case 2, there is a redistribution of strain (ε_i^+) by the collapse of the first pore layer to guarantee the same strain before and after the collapse. The collapsed pores consist of a higher volume fraction of solid strut material than the intact pores, hence, the collapsed pore layer is represented by a spring with a higher stiffness (E_i^+) and thus a smaller strain than before. The total length L of the sample and the individual lengths L_i of the springs as well as the internal length Q_1 of

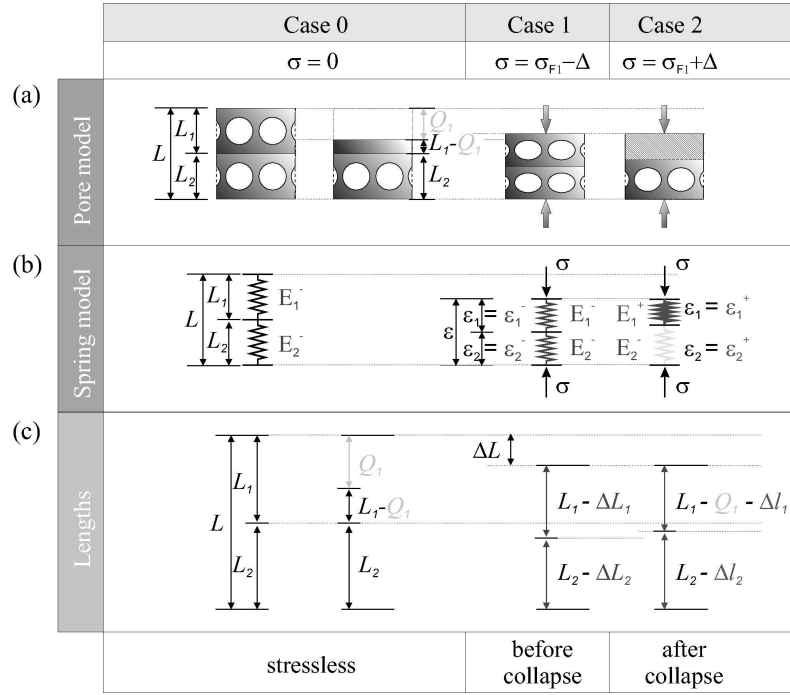


Figure 8: (a) Phenomenological pore model, (b) rheological spring model, (c) comparison of lengths.

pore layer 1 are represented in Figure 8 (c). In case 1 the total length variation ΔL is composed of the individual length variations ΔL_i whereas in the simplified case $\Delta L_1 = \Delta L_2$. Because of the fact that $L_1 - Q_1 + L_2$ is according to the second case of case 2, a stress-free state, after the pore collapse and the redistribution of strain, only Δl_i contribute to the evolution of stress, whereas spring 2 will be expanded and spring 1 will be compressed. Based on this, $\Delta l_1 > \Delta L_1$ and $\Delta l_2 < \Delta L_2$. For compatibility reasons one has

$$L_1 - \Delta L_1 + L_2 - \Delta L_2 = L_1 - Q_1 - \Delta l_1 + L_2 - \Delta l_2. \quad (2)$$

Hence, the length variation ΔL and strain ε under compression denot to

$$\Delta L = \Delta L_1 + \Delta L_2 = Q_1 + \Delta l_1 + \Delta l_2 \quad | : L \quad (3)$$

$$\varepsilon = \varepsilon_1^- + \varepsilon_2^- = \Omega_1 + \varepsilon_1^+ + \varepsilon_2^+. \quad (4)$$

A general constitutive equation can be developed by the considerations before and after pore collapse.

$$\text{Compatibility } \varepsilon = \varepsilon_1^- + \varepsilon_2^- = \Omega_1 + \varepsilon_1^+ + \varepsilon_2^+ \quad (5)$$

The left side, where the parameters are labeled with a superscript '-', denotes to the state before the pore collapse and the right side with parameters, labeled with a superscript '+', belongs to the state after the collapse. The

constitutive equations (see equations (14) and (15)) of the total foam system for both states are developed by the combination of the compatibility relation of equation (5) and Hooke's material law for a single pore in both states (see equations (6) - (9)).

$$\text{Single pore} \quad \sigma^- = E_i^- \varepsilon_i^- \quad (6) \quad \sigma^+ = E_i^+ \varepsilon_i^+ \quad (7)$$

$$\Rightarrow \varepsilon_i^- = \frac{1}{E_i^-} \sigma^- \quad (8) \quad \varepsilon_i^+ = \frac{1}{E_i^+} \sigma^+ \quad (9)$$

$$\text{Total system} \quad \varepsilon = \sum_{i=1}^n \varepsilon_i^- \quad (10) \quad \varepsilon - \sum_{i=1}^m \Omega_i = \sum_{i=1}^n \varepsilon_i^+ \quad (11)$$

$$\Rightarrow \varepsilon = \sum_{i=1}^n \frac{1}{E_i^-} \sigma^- \quad (12) \quad \varepsilon - \sum_{i=1}^m \Omega_i = \sum_{i=1}^n \frac{1}{E_i^+} \sigma^+ \quad (13)$$

$$\Rightarrow \sigma^- = \frac{1}{\sum_{i=1}^n \frac{1}{E_i^-}} \varepsilon \quad (14) \quad \sigma^+ = \frac{1}{\sum_{i=1}^n \frac{1}{E_i^+}} \left(\varepsilon - \sum_{i=1}^m \Omega_i \right) \quad (15)$$

The terminal values n and m of the summation variable label the total number of pores in the load direction and the number of collapsed pores, respectively. In general, equations (14) and (15) can be summarized by

$$\sigma = \frac{1}{\sum_{i=1}^n \frac{1}{E_i}} \left(\varepsilon - \sum_{i=0}^m \Omega_i \right), \quad (16)$$

whereas E_i is the actual stiffness of each pore layer

$$\sum_{i=1}^n \frac{1}{E_{tot}} = \sum_{i=1}^n \frac{1}{E_i} \quad (17)$$

Under the assumption of equal pore stiffnesses E^- for intact pores and equal stiffnesses E^+ for collapsed pores, there is the following case differentiation of the total Young's modulus E_{tot} of the foam

$$E_{tot} = \begin{cases} \frac{E^- E^+}{(n-m) E^+ + m E^-}, & \text{if } \varepsilon_{t+1} > \varepsilon_t \quad \text{or} \quad \varepsilon_{t+1} < \varepsilon_t \wedge m = 0 \\ 0, & \text{if } \varepsilon_{t+1} < \varepsilon_t \wedge m \geq 1 \\ E_{bulk}, & \text{if } m = n. \end{cases} \quad (18)$$

The phenomenological parameters Q_i and Ω_i are not pure fundamental mathematical parameters, but they can rather be motivated by the microstructure of the foams similar to the micro-macro identification process to model fluid-saturated grounds by Dell'Isola et al. (1998). An intact pore layer consists of solid struts and the pore fluid, mostly air. Hence, the volume V_{layer} of a pore layer can be separated into a solid volume V_{solid} of the struts and a pore volume V_{pore}

$$V_{layer} = V_{pore} + V_{solid} \quad (19)$$

The internal length Q_i can be microstructurally motivated as the length of the pore volume and as the length $L_{solid} = L_i - Q_i$ of the solid volume of an intact pore layer by conservation of the cross section A of the foam

under awareness of the foam mass m_{foam} or foam density ρ_{foam} , respectively and the bulk density ρ_{bulk} of the strut material.

$$Q_i = L_i - L_{solid} \quad (20)$$

$$= L_i - \frac{m_{foam}}{\rho_{bulk} A} \quad (21)$$

$$= L_i - \frac{\rho_{foam}}{\rho_{bulk}} \quad (22)$$

By introducing the porosity P as

$$P = 1 - \frac{\rho_{foam}}{\rho_{bulk}} \quad (23)$$

Q_i can be evaluated as

$$Q_i = P L_i. \quad (24)$$

According to this, the maximal strain Ω_i of a pore layer is

$$\Omega_i = \frac{Q_i}{L} = \frac{L_i}{L} P. \quad (25)$$

Hence, by the knowledge of the porosity, the total sample length and the length of one single pore, it is possible to microstructurally motivate the phenomenological parameter of the model.

Under the two assumptions of equal pore stiffnesses and equal pore lengths, the constitutive equation (16) can be simplified as an extended Hooke's law

$$\sigma = E_{tot} (\varepsilon - \Omega_{tot}) \quad (26)$$

whereas E_{tot} is the effective Young's modulus of the foam for each deformation state and can be calculated by equation (18). Ω_{tot} is the amount of the maximal strain by the collapsed pores. It can be calculated by the assumption of equal pore lengths by

$$\Omega_{tot} = \sum_{i=1}^m \Omega_i = m\Omega = m \frac{L_i}{L} P. \quad (27)$$

Herein Ω_i denotes to the internal strain of an individual pore, Ω to the average individual strain, L_i to the average pore length and L is the total length of the sample. Further parameters which can be calculated by the knowledge of microstructurally sizes are the number of pores in load direction n and the number of collapsed pores m , whereas

$$n = \frac{L}{L_i} \quad (28)$$

and

$$m = \frac{\varepsilon}{\Omega}. \quad (29)$$

By the knowledge of the maximal number of pores in load direction n and the average internal strain Ω , the densification strain ε_d can be evaluated as

$$\varepsilon_d = n\Omega. \quad (30)$$

4.3 Implementation and Test of the Simplified Model

The abovementioned simplified model (see section 4.2, equation (26)) has been implemented in the open source code Python. The stress-strain response for different porosities, sample lengths and pore sizes have been investigated and are shown in Figure 9. The standard parameters used in this study are: $E^- = 500$ MPa, $E^+ = 5000$ MPa, $L_i = 4$ mm, $L = 40$ mm and $P = 90\%$. The variations in the different Figures are mentioned in the Figures themselves. Figure 9 (a) shows that the model is able to describe the stress oscillations and also the hardening effect with increasing strain. Further it depicts higher densification strains for increasing porosities. As presented in Figure 9 (b) the model shows the correct behaviour under load reversal and from the unloading parts the raise in the global

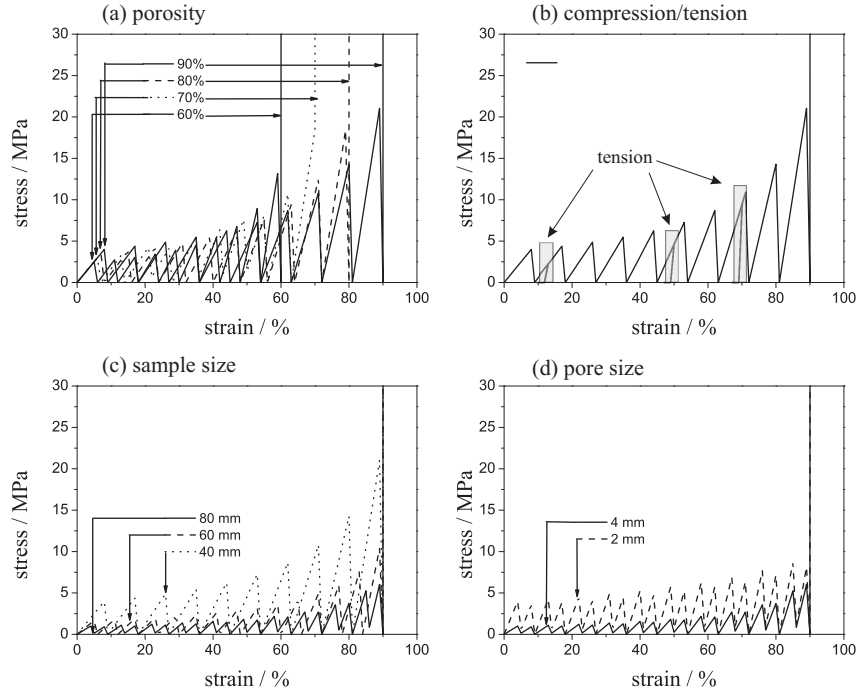


Figure 9: Investigation of the (a) porosity P , (b) load reversal, (c) sample length L and (d) pore size L_i

Young's modulus E_{tot} with increasing strain is visible. Furthermore, as outlined in Figure 9 (c), the simplified model is able to predict the qualitatively correct size effect by changing the sample size. Higher sample sizes lead to a weakening of the material response. The second kind of size effect, changes in the microstructural parameter of the pore size, will be accurately reflected (see Figure 9 (d)) if the Young's modulus E^- of the intact pore layer is corrected in close relation to the critical buckling load F_{crit} .

$$F_{crit} = \pi^2 \frac{EI}{L_i^2} \quad \Rightarrow \quad E^- \propto \frac{1}{L_i^2} \quad (31)$$

Hence, a reduction in the pore size which is correlated with a reduction in the critical buckling length ,e.g., by 50% leads to a four times larger Young's modulus E^- for intact pore layers. Considering this change in the stiffness, the model is able to predict the second kind of size effect, the weakening of the material response by increasing pore size, too.

5 Conclusions

In this study, open cell pure aluminum foams and Ni/Al hybrid foams have been characterised under uniaxial and biaxial loading, as well as under periodical unloading. The experimental observations such as different behavior under tensile and compressive loading, strain hardening, two kinds of size effects and the oszilating stress have been summerized in a simplified one-dimensional, microstructural motivated rheological spring model. The model has been implemented in Python and despite of its simplifications it is able to qualitatively decribe the experimental observations as well as the macroscopical material degradation by the mesoscopical damage of the foams. In future work there is the experimental determination of the model parameter and a three-dimensional extension of the model.

References

- Abrate, S.: Localized impact on sandwich structures with laminated facings. *Appl. Mech. Rev.*, 50, (1997), 69 – 82.
- Alibert, J.-J.; Seppecher, P.; Dell'Isola, F.: Truss modular beams with deformation energy depending on higher displacement gradients. *Mathematics and Mechanics of Solids*, 8, 1, (2003), 51–73.
- Andrews, E.; Gioux, G.; Onck, P.; Gibson, L.: Size effects in ductile cellular solids. part ii: experimental results. *Int. J. Mech. Sci.*, 43, (2001), 701 – 713.

- Ashby, M.: The mechanical properties of cellular solids. *Metall. Trans. A*, 14 A, (1983), 1755.
- Ashby, M. F.; Evans, A.; Fleck, N. A.; Gibson, L. J.; Hutchinson, J. W.; Wadley, H. N. G.: *Metal Foams: A Design Guide*. Butterworth-Heinemann, Oxford, Boston, Oxford (2000).
- Banhart, J.: Offenporige Aluminiumschäume – Eigenschaften und Anwendungen. *Aluminium*, 75, (1999), 1094 – 1099.
- Banhart, J.: Manufacture, characterisation and application of cellular metals and metal foams. *Prog. Mater. Sci.*, 46, (2001), 559 – U3.
- Banhart, J.; Baumeister, J.: Deformation characteristics of metal foams. *J. Mater. Sci.*, 33, (1998), 1431 – 1440.
- Banhart, J.; Baumeister, J.; Weber, M.: Aluminium foams for transport industry. *Mater. Design*, 18, (1997), 217 – 220.
- Chen, C.; Fleck, N.: Size effects in the constrained deformation of metallic foams. *J. Mech. Phys. Solids*, 50, (2002), 955 – 977.
- Dell’Isola, F.; Rosa, L.; Woniak, C.: A micro-structured continuum modelling compacting fluid-saturated grounds: The effects of pore-size scale parameter. *Acta Mechanica*, 127, 1-4, (1998), 165–182.
- Diebels, S.; Geringer, A.: Micromechanical and macromechanical modelling of foams: Identification of Cosserat parameters. *ZAMM-Journal of Applied Mathematics and Mechanics/Zeitschrift für Angewandte Mathematik und Mechanik*.
- Ferretti, M.; Madeo, A.; dell’Isola, F.; Boisse, P.: Modeling the onset of shear boundary layers in fibrous composite reinforcements by second-gradient theory.
- Jänicke, R.; Sehlhorst, H.-G.; Duster, A.; Diebels, S.: Micromorphic two-scale modelling of periodic grid structures. *International Journal for Multiscale Computational Engineering*, 11, 2.
- Jung, A.; Natter, H.; Diebels, S.; Lach, E.; Hempelmann, R.: Nanonickel coated aluminum foam for enhanced impact energy absorption. *Adv. Eng. Mater.*, 13, (2011), 23 – 28.
- Jung, A.; Natter, H.; Hempelmann, R.; Diebels, S.; Koblischka, M. R.; Hartmann, U.; Lach, E.: Electrodeposition of nanocrystalline metals on open cell metal foams: Improved mechanical properties. *ECS Transactions*, 25, (2010), 165 – 172.
- Jung, A.; Natter, H.; Hempelmann, R.; Lach, E.: Metal foams, EP 2261398 A1 (2009).
- Lefebvre, L.-P.; Banhart, J.; Dunand, D.: Porous metals and metallic foams: Current status and recent developments. *Adv. Eng. Mater.*, 10, (2008), 775 – 787.
- Onck, P.; Andrews, E.; Gibson, L.: Size effects in ductile cellular solids. part i: modeling. *Int. J. Mech. Sci.*, 43, (2001), 681 – 699.
- Tekoglu, C.; Gibson, L. J.; Pardoën, T.; Onck, P. R.: Size effects in foams: Experiments and modeling. *J. Appl. Phys.*, 56, (2011), 109 – 138.

Address: Anne Jung, Saarland University, Chair of Applied Mechanics, Campus A4.2, 66123 Saarbrücken
email: anne.jung@mx.uni-saarland.de